Desalination and Water Treatment
www.deswater.com

41 (2012) 170–178
March

doi: 10.1080/19443994.2012.664699

Taylor & Francis
Taylor & Francis Group

Adsorption of direct yellow 27 from water by poorly crystalline hydroxyapatite prepared via precipitation method

Khalid Mahmud[a], Md. Azharul Islam[b], Anastasios Mitsionis[a], Triantafillos Albanis[a], Tiverios Vaimakis[a,*]

[a]*Department of Chemistry, University of Ioannina, Ioannina 45110, Greece*
Tel. +30 2651008352; Fax: +30 2651008795; email: tvaimak@cc.uoi.gr
[b]*Forestry and Wood Technology Discipline, Khulna University, Khulna 9208, Bangladesh*

Received 5 July 2011; Accepted 9 January 2012

ABSTRACT

In the present study, hydroxyapatite powders were prepared by modified precipitation method and characterized by XRD, FT-IR and N_2 adsorption–desorption techniques. The prepared nonporous particles were organized to agglomerate with mesoporous structure and consisted of low crystallinity Ca-deficient hydroxyapatite and in amorphous phase. The commercial direct yellow 27 was selected as a model dye in order to examine the adsorption capacity of hydroxyapatite at room temperature. The adsorption isotherms are transformed from L-type to S-type curve, in Giles classification, by increasing the pH values. Equilibrium data fitted very well to the Langmuir model, signifying the energetic homogeneity of hydroxyapatite surface adsorption sites. The dye sorption kinetics was fairly described by the pseudo-first-order kinetic model.

Keywords: Hydroxyapatite; Direct yellow 27; Adsorption kinetics; Adsorption isotherms

1. Introduction

Modern society cannot ignore the grandness of dyes in everyday needs in an aesthetic point of view. Dyes are applied to numerous substrates, e.g. textiles, leather, cosmetics, plastics, paper, carpet etc., in order to bring colour into our lives. One of the main dye characteristics is that they must get completely or at least partially soluble in their containing substance and produce considerable amount of coloured waste water [1]. But certain kind of dyes can be toxic, carcinogenic or mutagenic and can pose a hazard to human health [2]. The nature of pollution that accompanies different textile- and dyeing-based industries is primarily due to the non-biodegradable nature of dyes along with strong presence of toxic trace metals, acid or alkali carcinogenic aromatic amines traceable in the effluents. The presence of these pollutants in aquatic systems reduces light penetration, which causes more slow photosynthetic activity and also has a tendency to chelate metal ions producing microtoxicity to fish and other organisms [3].

The removal of dyes before the effluents are discharged into water is of great importance and has always been a major problem due to the difficulty of treating such wastewaters by conventional methods [4]. Biological procedures, which are widely utilized in the dye removal, are very inefficient because of the low biodegradability of dyes [5]. To decontaminate dye-polluted wastewater, a variety of methods such as coagulation, chemical oxidation and reduction, photocatalysis, adsorption, ion pair extraction and electro-

*Corresponding author.

chemical techniques have been examined [6]. Adsorption techniques have been widely applied to the treatment of industrial wastewater containing dyes, heavy metals and other inorganic and organic impurities [4]. In some cases, it is possible to recover the adsorbed dye through desorption processes and reuse the large amounts of water employed by textile industries [7]. Activated carbon is widely used for the adsorption process due to its high adsorption capacity. However, its high cost sometimes tends to limit its use. Consequently, a number of low-cost adsorbents such as: peat [4], barro branco lutite [7], bottom ash [8], activated rice husks [9], red mud [10], carbon slurry [11,12], cyclodextrin-based material [13] activated slag [14], wheat husk [15,16] and used tea leaves [17] are being studied.

Hydroxyapatite (HA, $Ca_{10}(PO_4)_6(OH)_2$) is an important inorganic material in biology and chemistry [18,19]. Since many years, calcium phosphate materials were suitably used for a number of biomedical applications, e.g. artificial bone and teeth, as well as a carrier for drug delivery [20,21]. However, in the recent years, there has been an increasing interest for calcium phosphate materials as an adsorbent due to their ionic exchange property, adsorption affinity, characteristic to establish bonds with organic molecules, water insolubility, high stability under reducing and oxidizing conditions, availability and low cost [22,23]. There are many reports on HA usage to stabilize a variety of metals, such as Co, Pb, Cu, Zn, Cd, Sb, Cr [22–28]. The fluoride adsorption potential of novel nano-hydroxyapatite/chitin composite was also studied [29].

Moreover, recent reports suggest that HA surfaces show a good affinity for organic pollutants [30,31]. The ion exchange properties, adsorption affinity of the calcium phosphate materials as well as their characteristic to establish bonds with organic molecules of different sizes have made these materials to attract more attention during the last two decades. Despite its low specific surface area, they may be used as an efficient sorbent material for specific organic pollutants. Lin et al. [32] showed that the HA nanopowders exhibited good adsorption ability to phenol. Bouyarmane et al. [33] found strong interaction arising between pyridine and apatite surface, with comparable efficiency and lower processing costs than some activated carbons. The adsorption of methylene blue, basic yellow 28, reactive yellow 125 and disperse blue SBL textile dyes on apatite materials was also studied [34,35].

However, the influence of the HA morphology on dye adsorption has not yet been investigated. It is well known that mesoporous materials are highly desirable as they exhibit large specific surface area and suitable pore size.

Direct yellow 27 which is depicted in Fig. 1 is an anionic organic azo dye which can be found in many industrial wastes in aqueous environments. The interactions between the dye and the HA surface are of great importance. They may be attributed to the capability of HA to form a positively charged surface in slight acidic pHs. Therefore, the objective of this study is to investigate the removal of direct yellow 27 dye, from aqueous solution under different conditions, using HA as the "removing agent".

2. Materials and methods

2.1. Chemicals

All experiments were performed with analytical reagent grade chemicals and solvents. The reagents that have been used for the synthesis of adsorbent were $CaCl_2{\cdot}2H_2O$ (Fluka, Assay [KT] 99%), $Ca(H_2PO_4)_2{\cdot}H_2O$ (Riedel-de Haën, Assay 88%) and Ammonia solution 25% (Riedel-de Haën) as pH controller. Direct yellow 27 [$C_{25}H_{20}N_4Na_2O_9S_3$, Sigma-Aldrich. $\lambda_{max} = 398$ nm] was used as the dye tested for adsorption. The structure of direct yellow 27 is illustrated in Fig. 1. All solutions were prepared using distilled water from a borosilicate auto still (Jencons Ltd.).

2.2. Synthesis and characterization of HA

The apparatus used is described properly in our previous works [36]. A supersaturated solution was prepared by dissolving 0.0538 mol $Ca(H_2PO_4)_2{\cdot}H_2O$ and 0.1254 mol $CaCl_2$, with a Ca/P molar ratio of 1.67 (HA stoichiometry), into 800 mL of distilled water and then was transferred into the reactor vessel and was heated at 97 ± 1°C using an airflow rate of 15 L/h for 30 min. The rotation speed of the high speed dispersed equipment was adjusted at 5,000 rpm, and then 18 mL of concentrated NH_4OH solution (25% w/w) was added slowly (3 min). The pH of the solution increased from 3.8 to 8.8 and white slurry was produced. The produced slurry was aged over night at

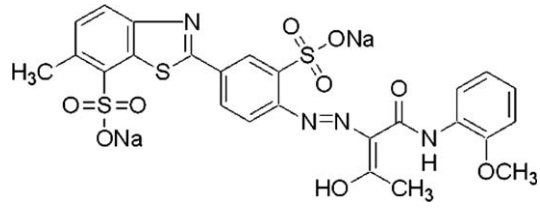

Fig. 1. Chemical structure of direct yellow 27.

room temperature, filtrated, washed using distilled water and dried at 90°C for 6 h.

The identification of the crystal phases in the obtained products was carried out by the X-ray diffraction (XRD) technique, using a Brüker P8 Advance apparatus, with a 2θ range of 20–50° in steps of 0.02° and the identification of the patterns was made using the powder diffraction files (PDF). FT-IR was performed using a spectrophotometer (Model Spectrum RX I FT-IR, Perkin–Elmer). KBr disk technique was used with 2 mg of powder in 200 mg of spectroscopic-grade KBr (Merck). Infrared spectra were recorded in the 4,000–400 cm^{-1} region.

The textural analysis of the solids was examined by N_2 adsorption–desorption porosimetry which also provides the pore size distribution, using Fisons Instruments Sorptomatic 1900. Before N_2 adsorption–desorption measurement, the sample was degassed at 150°C and in vacuum of 10–30 Torr for 6 h.

2.3. Adsorption experiments

An exact weighed quantity of dye was taken in a 500 mL flask and it was filled with double distilled water in order to make a stock solution of 500 mg/L (500 ppm). The stock solution was stored in a dark place at room temperature. All batch adsorption experiments were performed at room temperature and for this purpose 0.2 g of HA adsorbent (0.025– 0.300 g) was placed in a 50 mL polypropylene centrifuge tube containing 25.0 mL of dye solution (20–60 mg/L) at pH ranging from 3.5 to 11.5. Then, the tubes were shaken in a rotary orbital shaker (rotator drive STR4, UK) at 60 rpm for 3 h in order to reach equilibrium concentration. At the end of the shaking, the samples were centrifuged at 4,200 rpm for 5 min and the dye concentration of the supernatant was determined using a UV–visible spectrophotometer (Jasco, V-530, Japan).

The percentage of dye removal as well as the adsorbed amount was calculated by the following equations:

$$\text{Removal}\% = 100 \times \frac{(C_0 - C_e)}{C_0} \quad (1)$$

$$\text{Removal capacity } (q_e) = \frac{(C_0 - C_e) \cdot V}{m} \quad (2)$$

Where, q_e is the amount of dye taken up by the adsorbent (mg/g); C_0, the initial dye concentration (mg/L); C_e, the equilibrium concentration (mg/L); m, the adsorbent mass (g); and V, the volume (L) of the adsorption solution.

3. Results and discussion

3.1. Characterization of the HA

Fig. 2 shows the XRD pattern of HA powder. The sample has been first indexed with X-Cell algorithm [37] and refined afterwards with Pawley fitting in order to find the best approximation for the unit cell parameters. Background has been subtracted using a 20 points polynomial function and a smoothing function has been applied using Savitsky–Golay filter. The XRD pattern indicates both crystalline and amorphous HA phases. The sample yielded broad and overlapping reflections, indicating its low crystallinity. There is no other extraneous peak detected in XRD pattern, which indicates that the crystalline phase is single-phase HA. Peaks at 25.90° and 32.92° are assigned as major peaks of HA due to (0 0 2) and (3 0 0) planes [PDF 73-1731]. The lattice parameters were calculated using the X-Cell algorithm software. The calculated values are $a = 9.427$ Å, $c = 6.930$ Å and volume = 529.390 $Å^3$. These values are slightly different from the standard data of HA [PDF 73-1731], where $a = 9.400$ Å, $c = 6.930$ Å and volume = 530.30 $Å^3$. The difference of a-axis is due to the partial replaceent of PO_4 group by the acid phosphate group. According to LeGeros and LeGeros [38], the presence of acid phosphate group results in an increase in a- and b-axis, but on the contrary has no effect on the c-axis.

Fourier transform infrared spectroscopy (FT-IR) was used to characterize the synthesized HA. Fig. 3 shows the FT-IR absorption spectra of HA powder. According to the standard IR transmission spectra, peaks observed at 3,576 and 633 cm^{-1} are assigned to OH bands. Peaks around 472, 563, 960, 1,040 and 1,106 cm^{-1} can be attributed to phosphate groups (PO_4), and the peak at 873 cm^{-1} is assigned to P–O–H

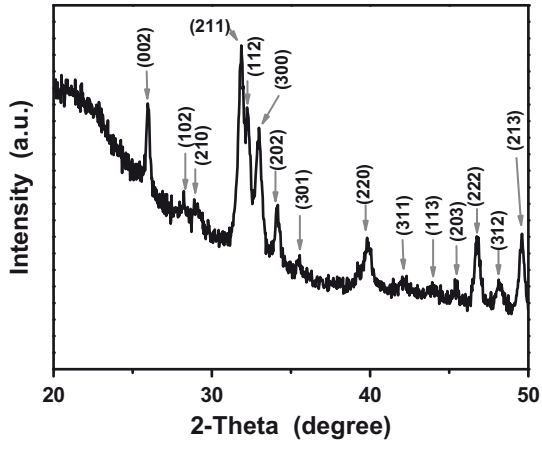

Fig. 2. XRD pattern of HA.

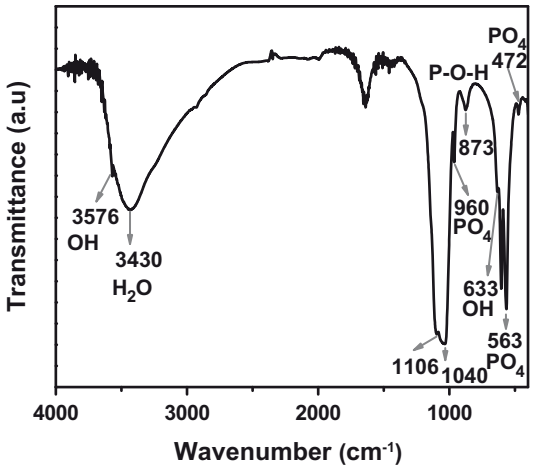

Fig. 3. FT-IR spectrum of HA.

bond. The presence of P–O–H bond indicates the Ca deficiency of the produced HA. The latter is in accordance with the XRD results.

The N_2 adsorption–desorption isotherms are shown in Fig. 4. The initial part of the adsorption isotherm ($P/P_0 < 0.2$) corresponds to monolayer adsorption that indicates a nonporous solid, according to the typical type II isotherm (IUPAC) [39]. The hysteresis loops, in the (P/P_0) range between 0.2 and 1.0, are similar to type H_3 (IUPAC), which indicates the appearance of mesopores due to the interspaces between the particles in the aggregates. A specific surface area of $53\,m^2/g$ was calculated according to the BET method [40].

3.2. Effect of dye solution pH

The pH is an important factor in the adsorption study, because it can influence both the structure of adsorbent, as well as the mechanism of adsorption. Both adsorbate and adsorbent may have functional groups, which are affected by the concentration of hydrogen (H^+) and hydroxyl ions (OH^-) in the solution. These ions are involved in the molecular adsorption process at the active sites of the adsorbent and are strongly dependent on the process of their treatments.

The percentage of dye adsorption was studied in a pH range between 3.5 and 11.5 and the results are shown in Fig. 5. The maximum adsorption is observed at pH 3.5. When, the solution pH increases from 3.5 to 6.5, the percentage of adsorption decreases slowly. Further increase of pH from 6.5 until 11.5, the adsorption of the dye decreases rapidly. According to Vucinic et al. [41], the sites that may form on the HA surface, depending on the conditions are positive ($\equiv Ca^+$, $\equiv HPO_4Ca^+$, $\equiv CaOH_2^+$, $\equiv OH_2^+$, etc.), neutral ($\equiv CaOH$, $\equiv PO_4Ca$, etc.) and negative ($\equiv PO_4^{2-}$, $\equiv HPO_4^-$, etc.). The same authors have concluded that in the pH range between 5.0 and 11.0 and especially in the alkaline range, HA particles have a negative zeta potential proving the adsorption of OH^- and HPO_4^{2-} ions. The latter comes from the dissolution process of HA surface thus new surface centers are formed ($\equiv HPO_4CaOH$, $\equiv HPO_4CaHPO$, etc.).

The variations of ζ-potential before and after adsorption of direct yellow 27 are shown in Fig. 6. The ζ-potential in all cases was negative. The value of ζ-potential of HA in the absence of dye at the pH range between 3.5 and 5.5 was about −20. In the same pH range, the negative value of the ζ-potential of HA after adsorption of the dye increased dramatically. At the pH range between 6.5 and 7.5, the ζ-potential of HA with and without dye was increased up to about

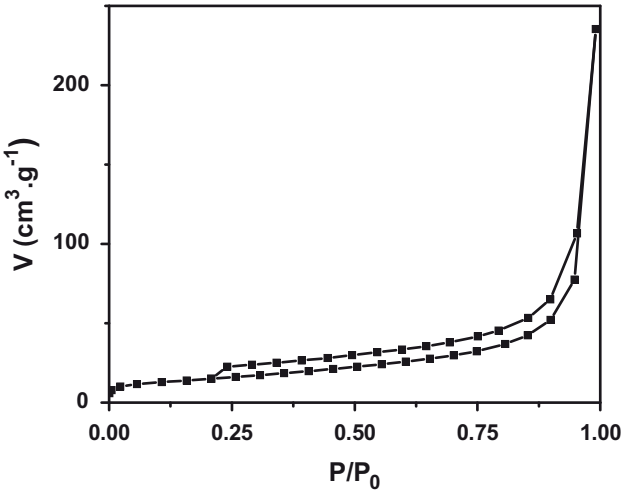

Fig. 4. N_2 adsorption–desorption isotherm of HA.

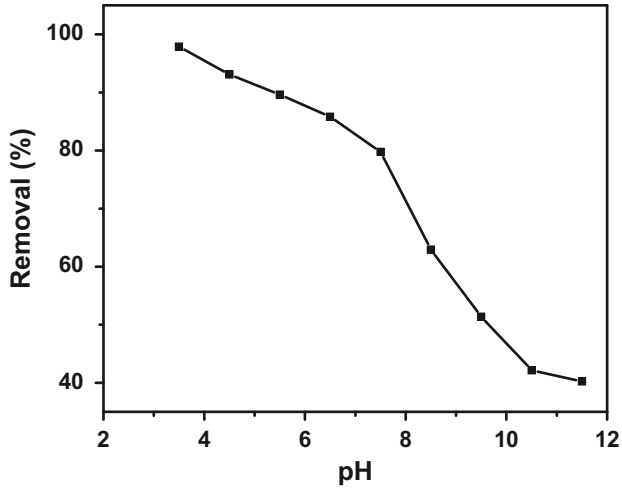

Fig. 5. Effect of pH on the removal of direct yellow 27 by HA (solution concentration: 40 mg/L, time: 180 min).

−35 as the pH increases. At high alkaline pH, the ζ-potential values remain around −38 in both cases.

Direct yellow 27 is an anionic dye chemically composed of sulfonated organic azo compounds which give sodium salts of sulfonic acids in aqueous solutions [42]. At lower pH, the main form of the dye is neutral in aqueous solution, thereby increasing the adsorption amount. On the contrary, by increasing the pH, the neutral form of dye changes into the negative ionic form and create inter-ionic repulsion between HA and dye as similarly charged particles. Thus, the extent of dye adsorption on the HA surface at basic pH is low. Similar behaviour has been observed for the adsorption of BSA protein [43] and Disperse Blue SBL [34] on HA and for reactive yellow 125 on natural phosphate [35].

3.3. Kinetic study

The most commonly used pseudo-first-order and pseudo-second-order models were employed to study the solid–liquid adsorption interactions. The first-order rate expression of Lagergren based on solid capacity [44] is generally expressed as follows in Eq. (3):

$$\log(q_e - q_t) = \log(q_e) - \frac{k_1 t}{2.303} \quad (3)$$

Whereas q_e and q_t (both in mg/g) are the amounts of dye adsorbed at equilibrium and at any time t, respectively, and k_1 (min^{-1}) is the adsorption rate constant. The values of k_1 were calculated from the slopes of the respective linear plots of $\log(q_e - q_t)$ vs. t. The intercept of the plot should be equal to $\log q_e$.

A pseudo-second-order model proposed by Ho and McKay [45] was used to explain the sorption kinetics. This model is based on the assumption that the adsorption follows second-order chemi-sorption. The pseudo-second-order model can be expressed as Eq. (4):

$$\frac{t}{q_t} = \frac{1}{k_2 q_e^2} + \frac{1}{q_e} t \quad (4)$$

Whereas k_2 ($g/mg\,min^{-1}$) is the rate constant of pseudo-second-order adsorption. The plot of t/q vs. t should give a linear relationship from which the constants q_e and k_2 can be determined.

The linear plot of pseudo-first- and second-order adsorption for an adsorbent amount of 0.2 g, distilled water pH and solution concentration of 20 and 40 mg/L are shown in Figs. 7 and 8, respectively. The rate constants, the calculated amounts of dye adsorbed at equilibrium, and the correlation coefficient are summarized in Table 1. The table shows that the correlation coefficient for both kinetic models is nearly equal to 1, however, the calculated values of q_e are better comparable to the experimental ones for the first-order model. Therefore, this section suggested that the pseudo-first-order model was the best choice to describe the adsorption behaviour of direct yellow 27 on HA particles.

3.4. Intra-particle diffusion rate constant

The rate constant for intra-particle diffusion of dye was obtained using Weber–Morris equation given as follows [46],

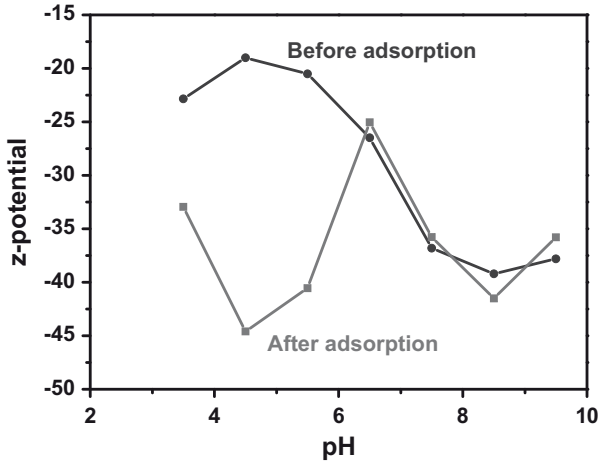

Fig. 6. Effect of pH on HA ζ-potential before and after the adsorption of direct yellow 27 (solution concentration: 40 mg/L, time: 180 min).

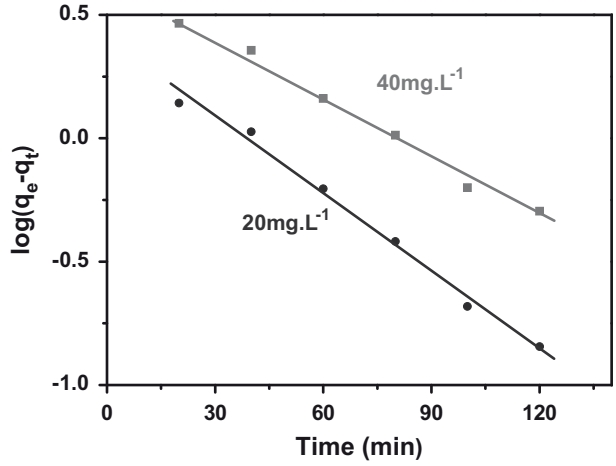

Fig. 7. First-order kinetics model of adsorption process (solution concentration: 20 and 40 mg/L, distilled water pH).

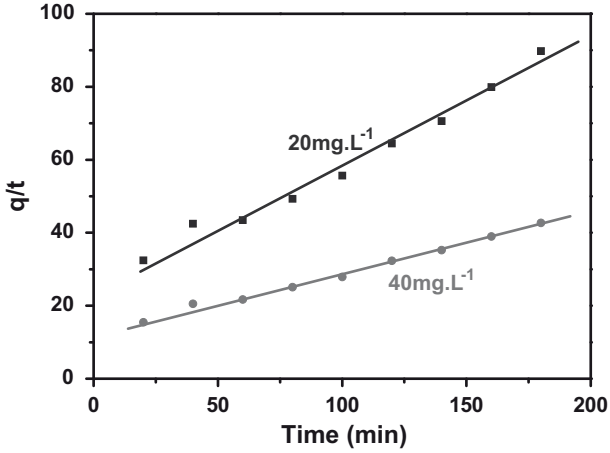

Fig. 8. Second-order kinetics model of adsorption process (solution concentration: 20 and 40 mg/L, distilled water pH).

Table 1
Kinetic constants for direct yellow 27 adsorption on HA

	Pseudo-first-order		Pseudo-second-order	
Concentration, mg/L	20	40	20	40
k	0.023	0.018	0.0048	0.0022
q_e (calculated)	2.50	4.42	2.92	6.04
q_e (experimental)	2.01	4.22	2.01	4.22
R^2	0.9914	0.9917	0.9803	0.9930

$$q = K_p t^{\frac{1}{2}} + C \quad (5)$$

Whereas q is the amount of direct yellow 27 adsorbed in mg/g of adsorbent, k_p is the intra-particle diffusion rate constant, and t is the agitation time in minutes. In order to determine the intra-particle diffusion rate constant in the adsorption process, the adsorbed amount of direct yellow 27q at anytime t was plotted as a function of square root of time ($t^{1/2}$). The values of k_p calculated from the slopes of the respective linear and the intercept of the plot should be equal to constant C. During the stirring, the adsorption of direct yellow 27 species takes place by adsorption at the outer surface of HA as well as there is a possibility of transport from the bulk into interspaces between the particles in the aggregates. The rate-limiting step may be either adsorption or intra-particle diffusion. The results obtained are presented in Table 2 and graphically shown in Fig. 9 for dye concentrations of 20 and 40 mg/L. It is evident from the graph that, the results were fitted by straight lines

Table 2
Intra-particle diffusion rate constants obtained from Weber–Morris equation for different initial concentrations of direct yellow 27

Initial concentration	Rate of pore diffusion (k_p)	C	R^2
20 mg/L	0.162	0.021	0.934
40 mg/L	0.333	0.004	0.965

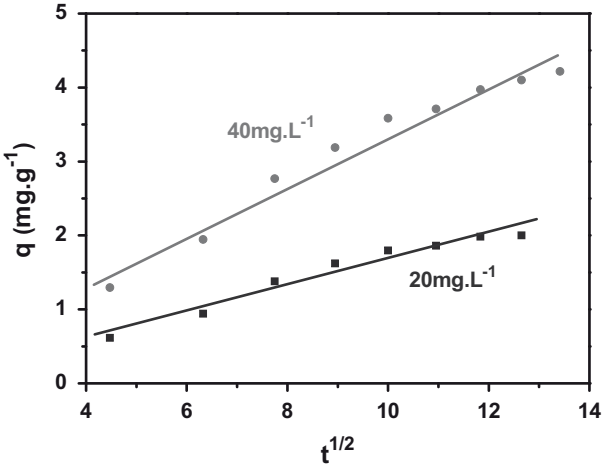

Fig. 9. Linear plot of Weber–Morris equation of direct yellow 27 removal by HA (solution concentration: 20 and 40 mg/L, distilled water pH).

with not very high values of the R^2, as well as, the y-intercept of the plots did not passing through the origin, thus indicating that intra-particle diffusion is not the sole rate-limiting mechanism for the adsorption of direct yellow 27 onto HA. In the present study, the intra-particle diffusion may be regarded as "concentration diffusion" because the values of k_p increase with the increase in direct yellow 27 concentration [47].

3.5. Adsorption isotherms

The adsorption equilibrium isotherm is an important factor for describing the way in which the adsorbate molecules can distribute between the liquid and the solid phases when the adsorption process reaches an equilibrium state. The amounts of adsorbed quantities of direct yellow 27 at the equilibrium (q_e) versus equilibrium dye concentration (C_e) for different pHs are drawn in Fig. 10. The adsorption isotherms for the pH values of 3.5, 4.5 and 5.5 are type L while for 6.5, 9.5 and 11.5 pH values are type S in Giles classification [48,49]. A type L curve may represent flatwise adsorbate orientation, while a type S one is usually

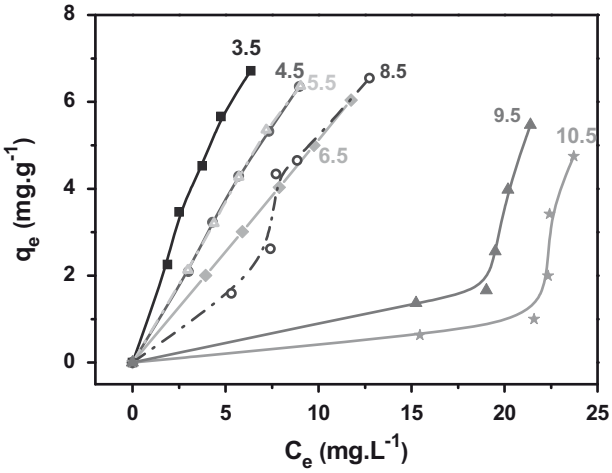

Fig. 10. Adsorption isotherm of direct yellow 27 onto HA. The initial pH values are indicated (solution concentration: 20, 30, 40, 50 and 60 mg/L, time 180 min).

taken to mean an end-on orientation. The S curve is generally the result of "cooperative adsorption", with solute molecules tending to be adsorbed packed in rows or clusters [50]. Type S isotherm appears when the binding energy of the first layer is lower than the binding energy between water molecules. In the acidic range of pH, the HA surface became positive and the two negative sulfonic groups of direct yellow 27 molecule are attached on the surface giving a flatwise orientation. Besides, in the same pH range, the protonated HA surface led to donor–acceptor interactions between the aromatic rings [51,32], enhancing the flatwise orientation. The increase of pH leads to the increasing of negative sites and therefore to the repulsion of sulfonic group from the HA surface, consequently, low adsorption affinity is observed. In the alkaline pH range, the –P–O$^-$ moieties on the HA surface and hydroxyl groups of direct yellow 27 molecule may interact via hydrogen bonding. In this case, we suggest an orientation of the adsorbed in which the molecules are stacked edge-on to the HA surface, with their main planes inclined at a low angle thereto, thus this arrangement permits cooperative adsorption [49]. The type S isotherm was also observed for the adsorption of reactive yellow 125 onto HA surface [35].

A theoretical approach [49] of the adsorption isotherms shows that we can move from an L-type to an S-type curve either by increasing E_{solute} or by increasing $E_{solvent}$: where E_{solute} and $E_{solvent}$ are the energy which the molecules of solute and solvent require before they lift off from the adsorbent surface and diffuse away into the solution. Assuming that the value of $E_{solvent}$ is independent of pH, we suggest that the E_{solute} is increased by increasing the pH.

Several equations are available in order to treat the isotherm adsorption results. Langmuir [52] and Freundlich [53] models are commonly used to describe the adsorption isotherm, and their constants afford significant parameters for predicting adsorption capacities.

The Langmuir equation is suitable to describe the adsorptive behaviour of homogeneous surfaces following the hypotheses: uniformly energetic adsorption sites, monolayer surface coverage and no interaction between adsorbed molecules.

Whereas, the Freundlich isotherm model assumes the heterogeneity of the surface, that is, the adsorption occurs at sites with different energies of adsorption. The energy of adsorption varies as a function of the surface coverage.

All the adsorption isotherms were constructed for used HA using the linearized Freundlich (Eq. (6)) and Langmuir (Eq. (7)) isotherm equations by plotting log (q_e) vs. log(C_e) and $1/q_e$ vs. $1/C_e$, respectively.

$$\log q_e = \log(K_F) + \frac{1}{n}\log(C_e) \tag{6}$$

$$\frac{1}{q_e} = \left(\frac{1}{K_a q_m}\right)\frac{1}{C_e} + \frac{1}{q_m} \tag{7}$$

where, q_e is the adsorbed amount (mg/g^{-1}), C_e is equilibrium concentration (mg/L), K_F is the Freundlich coefficient that represents the degree (strength) of adsorption. $1/n$ is an exponential coefficient that reflects the curvature in the isotherm. q_m (mg/g) is the maximum adsorption capacity of the adsorbent; K_a is the Langmuir's constant.

A list of the obtained parameters together with R^2 values is provided in Table 3. As seen, the equilibrium data are accommodated well by the Langmuir model (Fig. 11), with higher coefficient determination than the Freundlich model (Fig. 12). Such coefficient indicates that the monolayer coverage of the adsorbate (dye) is formed at the outer surface of the adsorbent (HA) with maximum adsorption capacity of 89.29 mg/g. The Freundlich model was able to describe sorption

Table 3
The adsorption parameters of Freundlich and Langmuir models

Freundlich			Langmuir		
K_F	$1/n$	R^2	q_m (mg/g)	K_a (l mg^{-1})	R^2
0.622	0.578	0.992	89.286	0.009	0.995

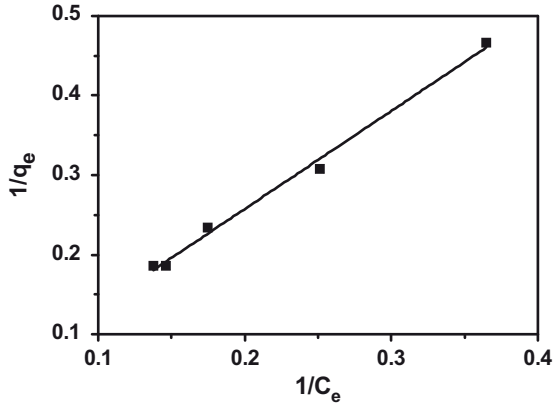

Fig. 11. Linear fit of experimental data obtained using Langmuir isotherm model.

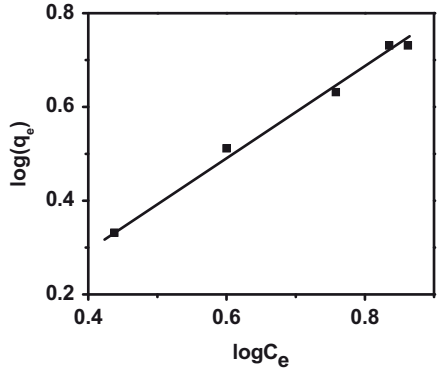

Fig. 12. Linear fit of experimental data obtained using Freundlich isotherm model.

isotherms for phenol using natural and synthetic apatites [33].

4. Conclusion

The phosphate materials prepared by modified precipitation method were composite of low crystallinity Ca-deficient HA and in amorphous phase. The observed particles were nonporous and spheroid in shape, which were organized to agglomerate as a mesoporous structure. The specific surface area was $53\,m^2/g$.

The adsorption decreases slowly as the solution pH increases up to 6.5. With further increase in pH, the adsorption decreases rapidly, due to change of neutral form of dye in negative ionic one, creating inter-ionic repulsion between negative HA particles.

The linear plot of Weber–Morris equation indicated that intra-particle diffusion is not the main rate-limiting mechanism. The overall process of direct yellow 27 adsorption on HA particles is best fitted by the pseudo-first-order model.

The Langmuir equation is suitable to describe the adsorptive behaviour, revealing the homogeneity of the HA surface with uniformly energetic adsorption sites, and monolayer surface coverage. The adsorption isotherms are moved from an L-type to an S-type curve, in Giles classification, by increasing the pH values, indicating that the adsorption from a flatwise adsorbate orientation, in acidic pH range, is converted to an edge-on one, in alkaline pH range.

The utilization of HA as an adsorbent for the removal of direct yellow 27 dye is proposed to be an economical dye-removal technique due to its low production cost.

References

[1] G. Crini, Non-conventional low-cost adsorbents for dye removal, a review, Bioresour. Technol. 97 (2006) 1061–1085.
[2] G. McKay, Adsorption of dyestuffs from aqueous solutions with activated carbon I: Equilibrium and batch contact-time studies, J. Chem. Technol. Biotechnol. 32 (1982) 759–772.
[3] G. McKay, M.S. Otterburn, A.G. Sweeney, The removal of colour from effluent using various adsorbents III.silica: Rate process, Water Res. 14 (1980) 15–20.
[4] A.N. Fernandes, C.A.P. Almeida, C.T.B. Menezes, N.A. Debacher, M.M.D. Sierra, Removal of methylene blue from aqueous solution by peat, J. Hazard. Mater. 144 (2007) 412–419.
[5] S. Preethi, A. Sivasamy, S. Sivanesan, V. Ramamurthi, G. Swaminathan, Removal of safranin basic dye from aqueous solutions by adsorption onto corncob activated carbon, Ind. Eng. Chem. Res. 45 (2006) 7627–7632.
[6] T. Akar, T.A. Demir, I. Kiran, A. Ozcan, A.S. Ozcan, S. Tunali, Biosorption potential of Neurospora crassa cells for decolorization of Acid Red 57 (AR57) dye, J. Chem. Technol. Biotechnol. 81 (2006) 1100–1106.
[7] C.A.P. Almeida, C. Machado, N.A. Debacher, Adsorption of methylene blue as a model for the use of barro branco as an alternative adsorbent for colour removal, Prog. Colloid. Polym. Sci. 128 (2004) 278–282.
[8] V.K. Gupta, I. Ali, V.K. Saini, T.V. Gerven, B.V. der Bruggen, C. Vandecasteele, Removal of dyes from wastewater using bottom ash, Ind. Eng. Chem. Res. 44 (2005) 3655–3664.
[9] V.K. Gupta, A. Mittal, R. Jain, M. Mathur, S. Sikarwar, Adsorption of Safranin-T from wastewater using waste materials—activated carbon and activated rice husk, J. Colloid Interf. Sci. 303 (2006) 80–86.
[10] V.K. Gupta, Suhas, I. Ali, V.K. Saini, Removal of rhodamine B, fast green and methylene blue from wastewater using red mud—an aluminum industry waste, Ind. Eng. Chem. Res. 43 (2004) 1740–1747.
[11] A.K. Jain, V.K. Gupta, A. Bhatnagar, Suhas Utilization of industrial waste products as adsorbents for the removal of dyes, J. Hazard. Mater. 101 (2003) 31–42.
[12] V.K. Gupta, R. Jain, S. Varshney, Removal of Reactofix golden yellow 3 RFN from aqueous solution using wheat husk—an agricultural waste, J. Hazard. Mater. 142 (2007) 443–448.
[13] G. Crini, H.N. Peindy, Adsorption of C.I. basic blue 9 on cyclodextrin-based material containing carboxylic groups, Dyes Pigments 70 (2006) 204–211.
[14] V.K. Gupta, S.K. Srivastava, D. Mohan, Equilibrium uptake, sorption dynamics, process optimization, and column operations for the removal and recovery of malachite green from wastewater using activated carbon and activated slag, Ind. Eng. Chem. Res. 36 (1997) 2207–2218.

[15] V.K. Gupta, R. Jain, S. Varshney, V.K. Saini, Removal of reactofix Navy Blue 2 GFN from aqueous solutions using adsorption techniques, J. Colloid Interf. Sci. 307 (2007) 323–332.
[16] V.K. Gupta, I. Ali, V.K. Saini, Adsorption studies on the removal of vertigo blue 49 and orange DNA13 from aqueous solutions using carbon slurry developed from a waste material, J. Colloid Interf. Sci. 315 (2007) 87–93.
[17] M.A. Islam, Z. Nikoloutsou, V. Sakkas, M. Papatheodorou, T. Albanis, Statistical optimization by combination of response surface methodology and desirability function for removal of azo dye from aqueous solution, Int. J Env. Ana. Chem. 90 (2010) 495–507.
[18] J.C. Elliott, Structure and chemistry of the apatite and other calcium, in: Studies in Inorganic Chemistry, vol. 18, Elsevier, Amsterdam, 1994, p. 111.
[19] R.Z. LeGeros, Calcium Phosphates in Oral Biology, Monographs in Oral Sciences, Vol 15 Myers H (ed), Karger, Basel, 1991.
[20] A. Barroug, M.J. Glimcher, Hydroxyapatite crystals as a local delivery system for cisplatin: Adsorption and release of cisplatin in vitro, J. Orthop. Res. 20 (2002) 274–280.
[21] M.R. Cannon, P.K. Bajpai, Continuous delivery of azidothymidine by hydroxyapatite or tricalcium phosphate ceramics, Biomed. Sci. Instrum. 31 (1995) 159–164.
[22] A. Krestou, A. Xenidis, D. Panias, Mechanism of aqueous uranium(VI) uptake by hydroxyapatite, Miner. Eng. 17 (2004) 373–381.
[23] Y. Feng, J.-L. Gong, G.-M. Zeng, Q.-Y. Niu, H.-Y. Zhang, C.-G. Niu, J.-H. Deng, M. Yan, Adsorption of Cd(II) and Zn (II) from aqueous solutions using magnetic hydroxyapatite nanoparticles as adsorbents, Chem. Eng. J. 162 (2010) 487–494.
[24] I. Smiciklas, S. Dimovic, I. Plecas, M. Mitric, Removal of Co^{2+} from aqueous solutions by hydroxyapatite, Water Res. 40 (2006) 2267–2274.
[25] A. Corami, S. Mignardi, V. Ferrini, Copper and zinc decontamination from single- and binary-metal solutions using hydroxyapatite, J. Hazard. Mater. 146 (2007) 164–170.
[26] Y. Xu, F.W. Schwartr, Sorption of Zn^{2+} and Cd^{2+} on hydroxyapatite surfaces, Environ. Sci. Technol. 28 (1994) 1472–1480.
[27] Q.Y. Ma, S.J. Tralna, T.J. Logan, J.A. Ryan, Effects of aqueous Al, Cd, Cu, Fe(II), Ni, and Zn on Pb immobilization by hydroxyapatite, Environ. Sci. Technol. 28 (1994) 1219–1228.
[28] B. Sandrine, N. Ange, B.-A. Didierb, C. Eric, S. Patric, Removal of aqueous lead ions by hydroxyapatites: Equilibria and kinetic processes, J. Hazard. Mater. 139 (2007) 443–446.
[29] C.S. Sundaram, N. Viswanathan, S. Meenakshi, Fluoride sorption by nano-hydroxyapatite/chitin composite, J. Hazard. Mater. 172 (2009) 147–151.
[30] A. Laghzizil, M. Mekkaoui, M. Ferhat, P. Barboux, Sorption of tribenuron-methyl onto apatite minerals, Toxicol. Environ. Chem. 81 (2001) 9–15.
[31] A. Bahdod, S. El Asri, A. Saoiabi, T. Coradin, A. Laghzizil, Adsorption of phenol from an aqueous solution by selected apatite adsorbents: Kinetic process and impact of the surface properties, Water Res. 43 (2009) 313–318.
[32] K. Lin, J. Pan, Y. Chen, R. Cheng, X. Xu, Study the adsorption of phenol from aqueous solution on hydroxyapatite nanopowders, J. Hazard. Mater. 161 (2009) 231–240.
[33] H. Bouyarmane, S. El Asri, A. Rami, C. Roux, M.A. Mahly, A. Saoiabi, T. Coradin, A. Laghzizil, Pyridine and phenol removal using natural and synthetic apatites as low cost sorbents: Influence of porosity and surface interactions, J. Hazard. Mater. 181 (2010) 736–741.
[34] N. Barka, S. Qourzal, A. Assabbane, A. Nounah, Y. Aitichou, Adsorption of disperse blue SBL dye by synthesized poorly crystalline hydroxyapatite, J. Environ. Sci. 20 (2008) 1268–1272.
[35] N. Barka, A. Assabbane, A. Nounah, L. Laanab, Y. Aît Ichou, Removal of textile dyes from aqueous solutions by natural phosphate as a new adsorbent, Desalination 235 (2009) 264–275.
[36] G.C. Koumoulidis, T.C. Vaimakis, A.T. Sdoukos, N.K. Boukos, C.C. Trapalis, Preparation of hydroxyapatite lath-like particles using high-speed dispersing equipment, J. Am. Ceram. Soc. 84 (2001) 1203–1208.
[37] M. Neumann, X-Cell—a novel indexing algorithm for routine tasks and difficult cases, J. Appl. Crystallogr. 36 (2003) 356–365.
[38] R.Z. LeGeros and J.P. LeGeros, Dense hydroxyapatite, in: Hench LL., Wilson J (Eds.), An Introduction to Bioceramics, World Scientific, London, 1993, pp. 139–180.
[39] S.J. Gregg, K.S.W. Sing, Adsorption, Surface Area, and Porosimetry, second ed., Academic Press, London, UK, 1982, p. 248.
[40] S. Brunauer, H.P. Emmett, E. Teller, Adsorption of gases in multimolecular layers, J. Am. Chem. Soc. 60 (1938) 309–319.
[41] D.R. Vucinic, D.S. Radulovic, S.D. Deusic, Electrokinetic properties of hydroxyapatite under flotation conditions, J. Colloid Interf. Sci. 343 (2010) 239–245.
[42] C.P. Kaushik, R. Tuteja, N. Kaushik, J.K. Sharma, Minimization of organic chemical load in direct dyes effluent using low cost adsorbents, Chem. Eng. J. 155 (2009) 234–240.
[43] G. Yin, Z. Liu, J. Zhan, F. Ding, N. Yuan, Impacts of the surface charge property on protein adsorption on hydroxyapatite, Chem. Eng. J. 87 (2002) 181–186.
[44] S. Lagergren, Zur theorie der sogenannten adsorption gelöster stoffe, Kungliga Svenska Vetenskapsakademiens, Handlingar Band 24 (1898) 1–39.
[45] Y.S. Ho, G. Mckay, The kinetics of sorption of basic dyes from aqueous solution by sphagnum mass peat, Can. J. Chem. Eng. 76 (1998) 822–827.
[46] M. Islam, P.C. Mishra, R. Patel, Physicochemical characterization of hydroxyapatite and its application towards removal of nitrate from water, J. Environ. Manage. 91 (2010) 1883–1891.
[47] K. Kadirvelu, C. Faur-Brasquet, P. LeCloiree, Removal of Cu (II), Pb(II) and Ni(II) by adsorption onto activated carbon cloths, Langmuir 16 (2000) 8404–8409.
[48] C.H. Giles, T.H. McEwan, D. Smith, Studies in adsorption Part XI. A system of classification of solution adsorption isotherms, and its use in diagnosis of adsorption mechanisms and in measurement of specific surface areas of solids, J. Chem. Soc. 11 (1960) 3973–3993.
[49] C.H. Giles, D. Smith, A. Huitson, A general treatment and classification of the solute adsorption isotherm (I), J. Colloid Interf. Sci. 47 (1974) 755–765.
[50] C.H. Giles, A.P. D'Silva, I.A. Easton, A general treatment and classification of the solute adsorption isotherm II. Experimental interpretation, J. Colloid Interf. Sci. 47 (1974) 766–778.
[51] X.L. Chai, Y.C. Zhao, Adsorption of phenolic compound by aged-refuse, J. Hazard. Mater. 137 (2006) 410–417.
[52] I. Langmuir, The constitution and fundamental properties of solids and liquids. Part I. Solids, J. Am. Chem. Soc. 38 (1916) 2221–2295.
[53] H. Freundlich, Uber die adsorption in losungen, Z. Phys. Chem. 57 (1906) 385–470.